Hyperfine structure of low-lying triplet states in ^{45}Sc II

A. Dockery,[1,2,*] K. König,[1] J. Lantis,[1,3] Y. Liu,[1] K. Minamisono,[1,2,†] S. Pineda,[1,3] and R. Powel[1,2]

[1]*Facility for Rare Isotope Beams, Michigan State University, East Lansing, Michigan 48824, USA*

[2]*Department of Physics and Astronomy, Michigan State University, East Lansing, Michigan 48824, USA*

[3]*Department of Chemistry, Michigan State University, East Lansing, Michigan 48824, USA*

(Received 9 August 2023; accepted 16 October 2023; published 17 November 2023)

Collinear laser spectroscopy experiments were performed on singly charged ^{45}Sc (^{45}Sc II). Fourteen fine-structure transitions in the $3d4s \leftrightarrow 3d4p$ configuration were studied for three sets of triplet states, the $^3D_1$, $^3D_2$, and $^3D_3$ states in the $3d4s$ configuration and the $^3F^o_2$, $^3F^o_3$, $^3F^o_4$, $^3D^o_1$, $^3D^o_2$, and $^3D^o_3$ states in the $3d4p$ configuration. Furthermore, the hyperfine magnetic dipole (A) and the electric quadrupole (B) coupling constants were determined. Detailed studies of experimental systematic uncertainties lead to accurate determination of the coupling constants and facilitate comparison with theoretical models, especially for B constants. The improved experimental uncertainty reveals deviations from available theoretical calculations and suggests the need for further theoretical studies.

DOI: 10.1103/PhysRevA.108.052816

I. INTRODUCTION

Detailed measurements of the hyperfine structure (HFS) of atomic energy levels are essential to benchmark atomic theories for nuclear structure studies of rare short-lived nuclei [1]. The magnetic dipole moment (μ) and the electric quadrupole moment (Q) of a short-lived nucleus can be extracted from the HFS magnetic dipole (A) and electric quadrupole (B) coupling constants. The magnetic moment is sensitive to the arrangement of nucleons inside a nucleus and the quadrupole moment is sensitive to its deformation, and thus the moments provide critical insights into the nuclear structure to be compared to modern nuclear theories. The magnetic dipole and electric quadrupole moments are typically obtained relative to a reference isotope of the same element, which requires the A and B coupling constants, as well as the nuclear moments, of the reference isotope to be known. However, when such reference isotope data are not available, the magnetic field and electric field gradient at the position of the nucleus must be calculated to extract the μ and Q from the A and B coupling constants, respectively. By comparing theoretical calculations to experimental results for A and B coupling constants, atomic theory calculations for the magnetic field and electric field gradients can be benchmarked to be used in the future measurements of electromagnetic moments of rare isotopes.

The A and B coupling constants are also vital in studies of element abundances in stellar systems [2]. Scandium, in particular, is important to these astrophysical studies as the lightest member of Fe-group elements. In studies of astrophysical data, the emission spectrum of Sc is spread out due to Doppler and rotational broadening [3]. This effect smears out the HFS in the emission lines, but if the HFS is not accurately accounted for, errors in stellar abundance estimates can be as large as 2 to 3 orders of magnitude [2]. Therefore, astrophysical studies rely on A and B coupling constants to be determined in laboratory experiments in order to accurately analyze the data. Some high-lying atomic states are not readily available for experimental measurement [2,4], so theoretical calculations must be used. Benchmarking atomic theory calculations of A and B coupling constants in low-lying states is important for an accurate calculation of these high-lying states.

Numerous studies have been performed on the coupling constants of ^{45}Sc in its neutral (^{45}Sc I) and singly charged (^{45}Sc II) states [2,4–9]. Recent experimental efforts have focused on ^{45}Sc I and high-lying ^{45}Sc II states [2,4]. Existing measurements on low-lying ^{45}Sc II states are several decades old, and some are contradicting. Here we provide measurements with high accuracy, taking advantage of modern experimental capabilities. The A and B coupling constants in ^{45}Sc II were measured for the $^3D_{1-3}$ states in the $3d4s$ configuration and $^3F^o_{2-4}$ and $^3D^o_{1-3}$ states in the $3d4p$ configuration. In particular, the accuracy of the B coupling constants was improved by a factor of 2 to 70 in the present study, enabling a meaningful comparison with theoretical calculations.

Atomic theory calculations for the ^{45}Sc II coupling constants have been performed in conjunction with experimental work [5,6,8,10,11]. Previous theoretical studies of ^{45}Sc II have largely utilized the multiconfiguration Dirac-Fock (MCDF) method [6,8]. However, MCDF calculations have struggled to reproduce the A coupling constants in ^{45}Sc II triplet states. In the present study, it is shown that MCDF calculations fail for many B coupling constants. The deviation from experimental results highlights the need for further theoretical work in ^{45}Sc II.

II. EXPERIMENT

Collinear laser spectroscopy (CLS) experiments were performed at the BEam COoling and LAser specotroscopy (BECOLA) facility [12,13] at the Facility for Rare Isotope

*dockery@frib.msu.edu
†minamiso@frib.msu.edu

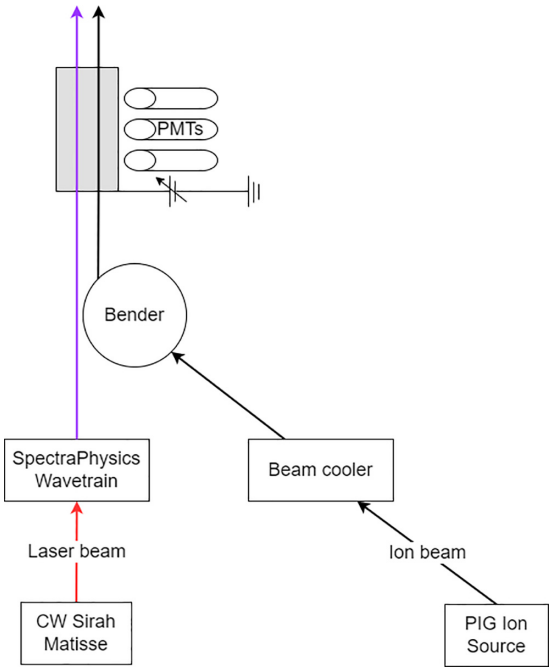

FIG. 1. A schematic showing the major components of the BECOLA experimental system as described in the text. The photon detection region (ellipsoidal reflectors) was on the scanning potential for the Doppler tuning of ion velocity.

Beams at Michigan State University. The experimental setup is shown schematically in Fig. 1. Singly charged ion beams of ^{45}Sc were produced by a Penning Ionization Gauge (PIG) ion source for offline beam production [14]. Ion beams were transported from the source to the BECOLA beamline and first passed through the radio-frequency quadrupole ion cooler [15], where ions were cooled through collisions with helium buffer gas to reduce the energy spread of the ion beam. Measurements were made with a typical ion current of 10 nA.

The ^{45}Sc beams were then accelerated to approximately 30 keV and entered the photon detection region, which was electronically isolated from the ground potential. Here, the ion beam energy was scanned by applying a small voltage to the photon detection region, which scanned the observed frequency in the 30-keV ^{45}Sc ion-beam frame via the Doppler shift. The laser frequency was fixed for a specific fine transition throughout the measurements. Typically, a hyperfine spectrum was obtained in 5- to 15-min intervals depending on the scatter of the hyperfine splitting. Five to 20 independent spectra were obtained on each transition.

The ^{45}Sc ions were excited for a specific transition in the photon detection region by overlapping the ion beam with a co- or counterpropagating laser light. Fundamental laser light was produced by a tunable continuous-wave (cw) Ti:sapphire ring laser (Sirah Matisse), which was locked to the readout of a wavemeter (HighFinesse WSU-30) that was actively calibrated against a frequency stabilized He-Ne laser (SIOS Meßtechnik GmbH). Typical frequency drift over a day measurement period was 1 MHz. The fundamental light was then frequency doubled (SpectraPhysics Wavetrain) for the spectroscopy. The typical laser power used for spectroscopy was 300 μW with a power fluctuation of less than 10^{-3}. Laser resonant photons were detected by three photomultiplier tubes (PMTs) in the detection region, which was on the scanning potential to Doppler tune the ion beam velocity. One detection system had an ellipsoidal reflector to collect resonant photons and spatially separate background photons on the surface of the PMT to enhance the signal-to-noise ratio [13]. The other two systems had an ellipsoidal reflector and a compound parabolic concentrator to have additional angular selection to eliminate background [16].

III. RESULTS

A. HFS spectra

The hyperfine coupling constants were extracted by fitting the hyperfine spectra from 14 different fine-structure transitions with a least-squares method. Example spectra are shown in Fig. 2 where the dashed blue lines are the result of the best fit to the data. A pseudo-Voigt profile was used to fit each peak in the hyperfine spectrum [Eq. (1)] [17], where C is the amplitude, μ is the center, α is the fraction of the Lorentzian component, and $2\sigma_{g,l}$ gives the full width at half maximum of the Gaussian and Lorentzian components respectively:

$$f(x : C, \mu, \sigma_g, \sigma_l, \alpha) = \frac{(1-\alpha)C}{\sigma_g}\sqrt{\frac{\ln(2)}{\pi}}e^{\frac{-(x-\mu)^2\ln(2)}{\sigma_g^2}} + \frac{\alpha C}{\pi}\frac{\sigma_l}{(x-\mu)^2+\sigma_l^2}. \quad (1)$$

The location of each hyperfine peak was fixed relative to the centroid by the energy shift [Eq. (2)] as a function of coupling constants of upper and lower states for the spectroscopy, so that the coupling constants were extracted from the fit:

$$\Delta E = \frac{K}{2}A + \frac{3K(K+1) - 4I(I+1)(J+1)}{8I(2I-1)(2J-1)}B. \quad (2)$$

Here, I is the nuclear spin, J is the total electron angular momentum, and F is the hyperfine quantum number defined by the vector sum $\mathbf{F} = \mathbf{I} + \mathbf{J}$. K is the quantum number given by $K = F(F+1) - I(I+1) - J(J+1)$, and A and B are the hyperfine coupling constants. The relative amplitude of each hyperfine peak was fixed in the analysis by evaluating the Wigner symbols, and the common dipole matrix element was left free as the overall scaling in the fitting procedure. This method is described in detail in Ref. [18].

B. Uncertainty evaluation

Due to the high statistics achievable in offline CLS measurements, systematic uncertainty is often the dominant source of uncertainty. Systematic uncertainties associated with the present measurements were studied in detail, and a quadratic sum of the four most significant sources was used as the systematic uncertainty for the coupling constants. This resulted in a total systematic uncertainty of 140 ppm for A coupling constants and 210 ppm for B coupling constants. Each contribution is discussed below.

(i) Beam energy. The ion beam energy in the present measurement was approximately 30 kV. By combining measurements of the same transition with copropagating (collinear) and counterpropagating (anticollinear) laser light,

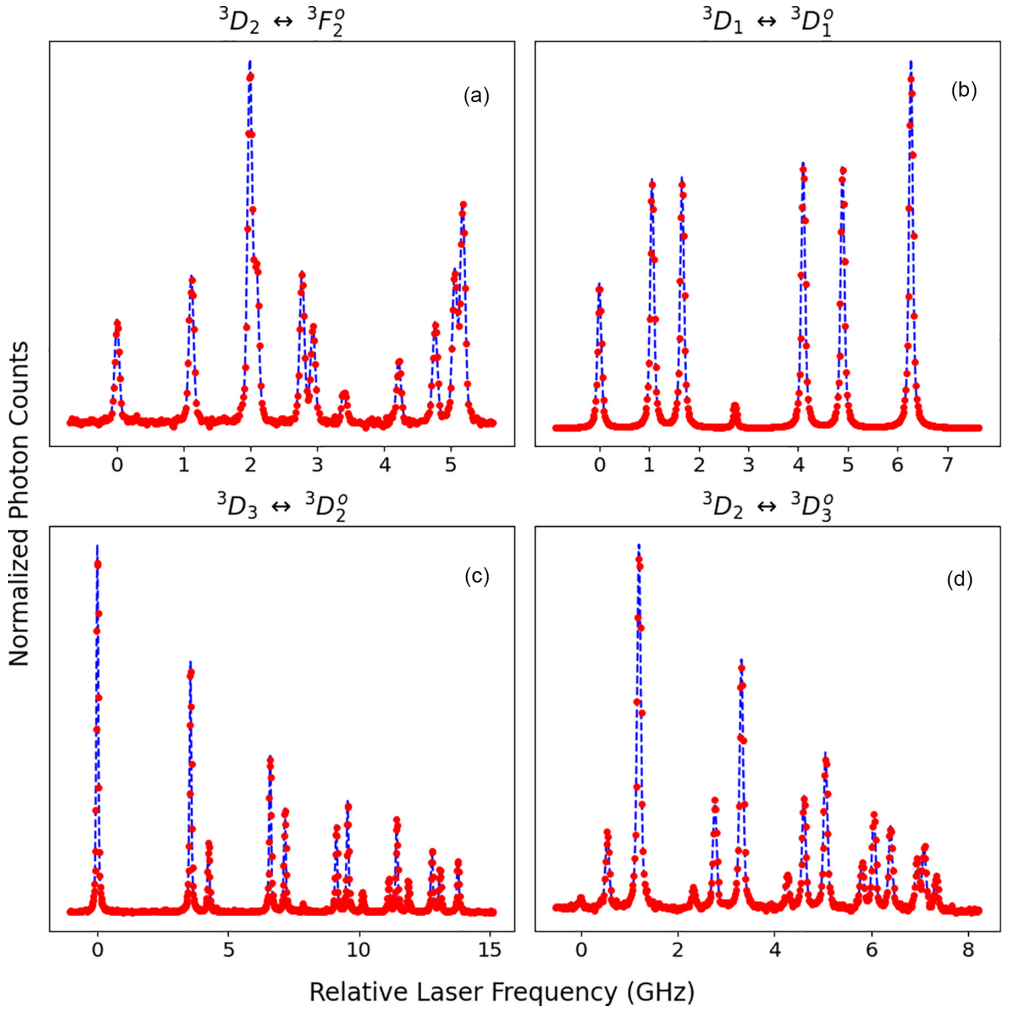

FIG. 2. Example spectra from four $3d4s$ to $3d4p$ fine structure transitions. Data points are shown by red points, and the fit is given by the dashed blue line. Frequency is reported relative to the first hyperfine peak in each spectrum.

the beam energy can be determined with high accuracy [19]. For Sc II, the collinear-anticollinear measurement was performed for the $^3D_2 \leftrightarrow {}^3F_3^o$ and $^3D_1 \leftrightarrow {}^3P_0^o$ fine-structure transitions, which were used as references to determine the beam energy of an individual measurement. These transitions were measured repeatedly over many days. Between those reference measurements, drifts of up to 1 eV are considered, which corresponds to a 20 ppm uncertainty for A coupling constants and a 40 ppm uncertainty for B coupling constants.

(ii) Beam deflection. The high voltage applied to the optical detection region acts like an electrostatic lens and, if misaligned relative to the ion beam, can cause deflections. As the applied voltages, up to 1.7 kV, are relatively large, a deflection of up to 1 mrad that depends on the scanning voltage was estimated, leading to an uncertainty of 80 ppm for A coupling constants and 120 ppm for B coupling constants.

(iii) Scan voltage. The digital voltmeter, used to measure the scanning voltage, had an uncertainty of 50 ppm. This leads to a 50 ppm uncertainty for A coupling constants and a 80 ppm uncertainty for B coupling constants.

(iv) Field penetration. The first PMT location in the photon detection region experiences an electric field penetration effect due to the geometry of the applied scanning potential. The field penetration was studied at BECOLA with Ca ions, which showed the applied potential was reduced by 550 ppm with an uncertainty of 100 ppm. The field penetration uncertainty corresponds to an uncertainty of 100 ppm for A coupling constants and 150 ppm for B coupling constants.

Statistical uncertainty for each measurement was given by the fit uncertainty, which was normalized by $\sigma_{\rm fit}\sqrt{\chi^2_{\rm dof}}$ when the $\chi^2_{\rm dof}$ was greater than 1. $\sigma_{\rm fit}$ is the uncertainty of the coupling constants from the regression, and $\chi^2_{\rm dof}$ is the best-fit χ^2 divided by the difference between the number of data points and free variables in the fit. The weighted mean of all measurements of a given hyperfine level was taken as the final result for the coupling constants, with the fit uncertainty used as the weight. The final statistical uncertainty is the quadratic sum of the propagated fit uncertainties and the standard error of the mean for the distribution of individual measurements.

C. *A* and *B* hyperfine coupling constants

Results of the A and B hyperfine coupling constants are summarized in Table I, together with literature values and theoretical calculations. In the table, the first set of parentheses is for the statistical uncertainty and the second set is for the

TABLE I. Experimental and theoretical hyperfine coefficients for the triplet states in Sc II considered in the present study. For measurements in this work, the one-σ statistical uncertainty is given in the first set of parentheses and the one-σ systematic uncertainty is given in the second set of parentheses.

State		A (MHz)			B (MHz)		
		This work	Literature	Theory	This work	Literature	Theory
$3d4s$	$^3D_1$	−479.51(2)(7)[a]	−480(1)[b]	−279.7[b]	−11.7(1)(0)[a]	−13(2)[b]	11.8[b]
				−473.3[c]			
	$^3D_2$	507.53(3)(7)[a]	510(1)[b]	453.4[b]	−32.5(2)(0)[a]	−30(6)[b]	−13[b]
				518.8[c]			
	$^3D_3$	656.73(2)(9)	654.8(3)[b]	608.5[b]	−45.4(3)(0)	−63(12)[b]	−35.5[b]
$3d4p$	$^3F_2^o$	367.94(3)(5)	366.8(11)[d]	425.3[b]	−54.7(2)(0)	−40(14)[d]	−31.7[b]
				309.2[d]			−47.9[d]
	$^3F_3^o$	205.61(3)(3)[a]	205.4(6)[d]	193.7[b]	−59.2(3)(0)[a]	−70(18)[d]	−58.5[b]
				193.8[d]			−52.2[d]
	$^3F_4^o$	102.23(3)(1)	102.3(1)[e]	115.6[b]	−84.0(9)(0)	−84(2)[e]	−76.0[b]
	$^3D_1^o$	304.98(3)(4)	307(1)[b]	267.7[b]	4.9(1)(0)	1(4)[b]	−0.7[b]
			304.7(2)[e]	278.3[d]		4.5(8)[e]	1.1[d]
			303.2(15)[d]	242[f]		10(5)[d]	10[f]
			304.3(4)[f]			2(2)[f]	
	$^3D_2^o$	124.95(3)(2)	125.7(2)[b]	149.0[b]	4.8(3)(0)	6(2)[b]	−11.7[b]
			125.3(1)[e]	165.5[d]		10(1)[e]	−4.7[d]
			125.4(5)[f]	130[f]		7(4)[f]	14[f]
	$^3D_3^o$	99.64(3)(1)	101.8(3)[b]	128.3[b]	13.6(5)(0)	24(5)[b]	−13.1[b]
			99.5(1)[e]	134.4[d]		21(2)[e]	−5.5[d]
			101.4(4)[f]	93[f]		−23(6)[f]	28[f]

[a]Reference [9].
[b]Reference [8]. Note, two σ error bars were reported, so uncertainty was halved for comparison in this table.
[c]Reference [8]. Alternative calculation using a polarized core.
[d]Reference [6].
[e]Reference [7]. Note that error bars were ambiguous when compared to Ref. [6], so the interpretation in Ref. [8] was used.
[f]Reference [5]. Note, two-σ error bars were reported, so uncertainty was halved for comparison in this table.

systematic uncertainty. Results are also shown in Figs. 3 and 4 for the A and B coupling constants, respectively. Literature values and theoretical calculations are shown relative to the present result. Unless they are shown as a gray bar, the total uncertainties of the present results are within the dashed line at 0. Note the variation of the scale of y axes. In particular, the scatter of literature and theoretical calculations for the B coupling constants is large, highlighting the accurate determination of the present results.

IV. DISCUSSION

Previous measurements of the low-lying states in ^{45}Sc II were made with the CLS technique. Early works used optical spectroscopy from metastable $3d^2$ states to probe the $3d4p$ configuration. First, the $^3D^o_{1-3}$ states in the $3d4p$ configuration were measured [5], which was later expanded on with a remeasurement of the $^3D^o_1$ state and a first time measurement of the $^3F^o_{2,3}$ states in the $3d4p$ configuration [6]. Later, the laser-rf double-resonance (LRDR) technique was used to precisely measure the $3d^2$ configuration [7]. The $^3F^o_4$ and $^3D^o_{1-3}$ states in the $3d4p$ configuration were determined by the same optical spectroscopy technique, but the ground-state coupling constants were fixed to the LRDR results. In the most recent measurements, the $^3D_{1-3}$ states in the $3d4s$ configuration and the $^3D^o_{1-3}$ states in the $3d4p$ configuration were measured by conventional CLS [8].

Our results determine the A coupling constants to smaller statistical uncertainty than the previous measurements as shown in Fig. 3(b). We also resolve the discrepancies between independent literature values for the $^3D^o_{1,3}$ states in the $3d4p$ configuration. Because of the high statistical accuracy achieved for the A coupling constants, we present the analysis of systematic uncertainty to provide reliable results. Additionally, the high statistics reported here for B coupling constants allows for meaningful tests of the predictions of atomic theory in the $3d4s$ and $3d4p$ configurations. Previous measurement for B coupling constants are compared in Fig. 4(b), which highlights the accuracy of this work.

Theoretical works on ^{45}Sc II began for states in the $3d^2$ and $3d4p$ configurations [5,10]. The calculations assumed perfect LS coupling and no contribution of configuration interaction (CI) or core polarization (CP) effects. Later efforts utilized the MCDF calculations [6,8]. This method, described in Ref. [11], accounts for CI effects but does not introduce any CP dependence. The technique was applied throughout the $3d^2$ and $3d4p$ configurations [6]. These calculations were later repeated and extended to the $3d4s$ configuration [8]. Notably, the two independent calculations yielded different values for many states, as seen in Figs. 3(a) and 4(a).

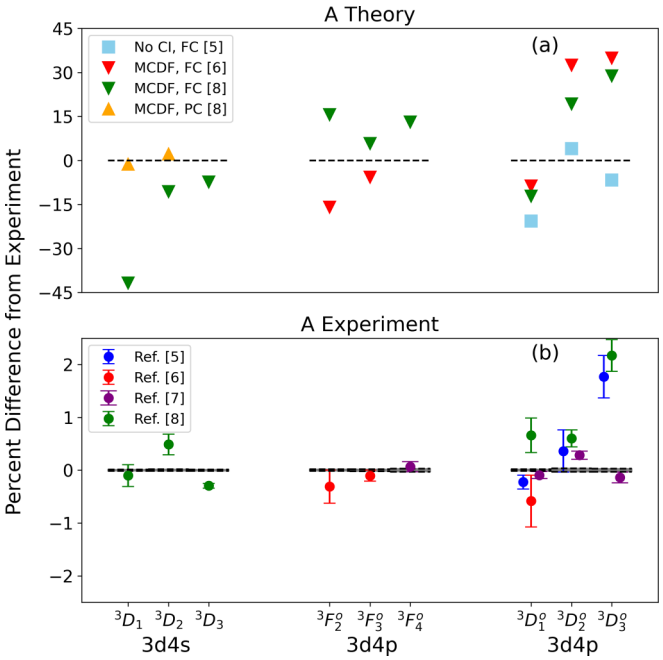

FIG. 3. In panel (a), the percent difference of theoretical calculations from this experiment are plotted for A coupling constants. Because of the scale of scatter, the error bars of experimental measurements are not visible outside of the line drawn at 0. Theoretical calculations are identified by their type, MCDF or no configuration interaction (CI) considerations, and their treatment of the electronic core as a frozen core (FC) or a polarized core (PC). In panel (b), previous measurements are evaluated with the same percent difference calculation. An error band corresponding to the quadratic sum of the statistical and systematic uncertainties in our measurements is drawn around 0.

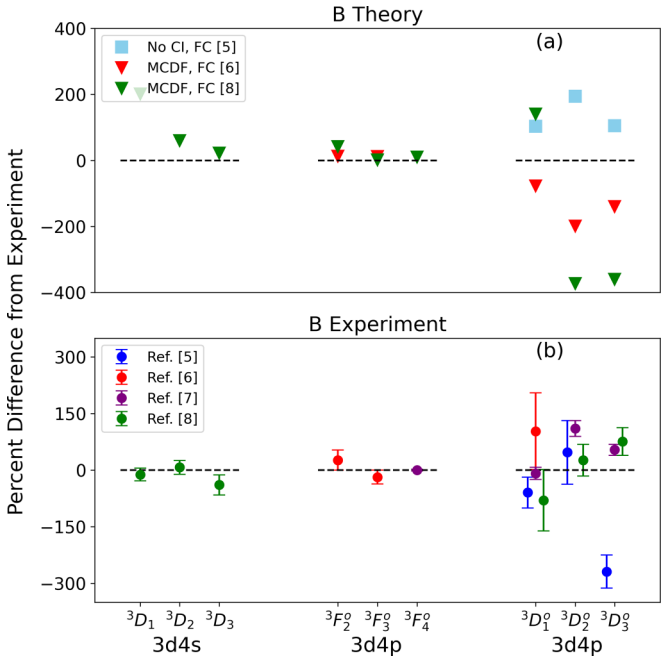

FIG. 4. An equivalent plot to Fig. 3 showing the percent difference for B coupling constants in (a) theoretical calculations and (b) previous measurements. The uncertainty of our measurements is not resolved outside of the line at 0 in the figures because of the y-axis scales.

Because of the low experimental precision on B coupling constants, the MCDF method was mainly evaluated on its agreement with A coupling constants. The method reproduced singlet states well, but struggled with triplet states, especially in the $3d4s$ and $3d^2$ configurations [6–8]. A modified MCDF method with polarized $3s$ and $3p$ core shells was introduced to account for the difference in the $3d4s$ $^3D_{1,2}$ A coupling constants [8]. However, the calculations were not extended to any other states.

Previously, atomic theory predictions of ^{45}Sc II B coupling constants could only be evaluated for the $3d^2$ configuration with the high-precision LRDR measurements [7]. The results showed good agreement between MCDF calculations and experiments for B coupling constants. As CP has a larger effect on A coupling constants than B, the agreement for B coupling constants suggested that the lack of CP consideration in the MCDF calculations was the source of the disagreement in A coupling constants. However, the measurements presented in this work show that MCDF predictions fail for B coupling constants in the $3d4s$ and $3d4p$ D series [see Fig. 4(a)]. Deviation beyond 100% is seen in four of six states and is often further from experiment than the no CI, frozen core calculations from Ref. [5]. Notably, the only D state measured with the LRDR method, the $3d^2$ $^1D_2$ state, also saw a deviation of nearly 100% from MCDF predictions [7]. Since the CP effect is small in B coupling constants, the large discrepancies suggest the disagreement between MCDF predictions and experiment stem from something else. The known deviations between available theoretical calculations and A coupling constants, combined with the large deviations in B coupling constants presented in this work, show that more theoretical work is needed for ^{45}Sc II.

V. CONCLUSION

Collinear laser spectroscopy experiments were performed on ^{45}Sc II. The A and B hyperfine coupling constants of the $^3D_{1-3}$ states in the $3d4s$ configuration and the $^3D^o_{1-3}$ and $^3F^o_{2-4}$ states in the $3d4p$ configuration were measured with 14 different fine-structure transitions. Detailed studies of experimental systematics were performed to accompany the accurate statistics achieved for the A and B coupling constants.

The improved accuracy on B coupling constants allows for a meaningful test of the atomic theory predictions in the $3d4s$ and $3d4p$ configurations. Large disagreement between experiment and MCDF calculations was found for the D-series B constants. Further theoretical work on ^{45}Sc II is needed to resolve these differences and would have direct applications to nuclear structure and astrophysical studies in this region.

ACKNOWLEDGMENTS

This work was supported by the National Science Foundation under Grant No. PHY-21-11185 and in part by the Michigan State University Honors College.

[1] X. F. Yang, S. J. Wang, S. G. Wilkins, and R. F. G. Ruiz, Prog. Part. Nucl. Phys. **129**, 104005 (2023).
[2] Hala and G. Nave, Astrophys. J. Suppl. Series **259**, 17 (2022).
[3] A. Abt, Astrophys. J. **115**, 199 (1952).
[4] Y. Xu, D. Fang, H. Fu, M. Liu, H. Ma, Z. Yang, Y. Yang, and Z. Dai, Eur. Phys. J. D **75**, 284 (2021).
[5] A. Arnesen, R. Hallin, C. Nordling, Ö. Staaf, L. Ward, B. Jelénkovi, M. Kisielinski, L. Lundin, and S. Mannervik, Astron. Astrophys. **106**, 327 (1982).
[6] L. Young, W. J. Childs, T. Dinneen, C. Kurtz, H. G. Berry, L. Engström, and K. T. Cheng, Phys. Rev. A **37**, 4213 (1988).
[7] N. B. Mansour, T. Dinneen, L. Young, and K. T. Cheng, Phys. Rev. A **39**, 5762 (1989).
[8] P. Villemos, R. van Leeuwen, A. Arnesen, F. Heijkenskjöld, A. Kastberg, M. O. Larsson, and S. A. Kotochigova, Phys. Rev. A **45**, 6241 (1992).
[9] R. Powel, B. A. Brown, J. D. Holt, A. Klose, K. König, J. Lantis, K. Minamisono, T. Miyagi, and S. Pineda, Phys. Rev. C **105**, 034310 (2022).
[10] M. G. Edmunds, Astron. Astrophys. **23**, 311 (1973).
[11] K. T. Cheng and W. J. Childs, Phys. Rev. A **31**, 2775 (1985).
[12] D. Rossi, K. Minamisono, B. R. Barquest, G. Bollen, K. Cooper, M. Davis, K. Hammerton, M. Hughes, P. F. Mantica, D. J. Morrissey, R. Ringle, J. A. Rodriguez, C. A. Ryder, S. Schwarz, R. Strum, C. Sumithrarachchi, D. Tarazona, and S. Zhao, Rev. Sci. Instrum. **85**, 09503 (2014).
[13] K. Minamisono, P. Mantica, A. Klose, S. Vinnikova, A. Schneider, B. Johnson, and B. Barquest, Nucl. Instrum. Methods Phys. Res. Sect. A **709**, 85 (2013).
[14] C. A. Ryder, K. Minamisono, H. B. Asberry, B. Isherwood, P. F. Mantica, A. Miller, D. M. Rossi, and R. Strum, Spectrochim. Acta Part B **113**, 16 (2015).
[15] B. R. Barqeust, G. Bollen, P. F. Mantica, K. Minamisono, R. Ringle, S. Schwarz, and C. Sumithrarachchi, Nucl. Instrum. Methods Phys. Res. Sect. A **866**, 18 (2017).
[16] B. Maaß, K. König, J. Krämer, A. J. Miller, K. Minamisono, W. Nörtershäuser, F. Sommer, arXiv:2007.02658.
[17] A. L. Stancik and E. B. Brauns, Vib. Spectrosc. **47**, 66 (2008).
[18] P. Siddons, C. S. Adams, C. Ge, and I. G. Hughes, J. Phys. B: At., Mol. Opt. Phys. **41**, 155004 (2008).
[19] K. König, K. Minamisono, J. Lantis, S. Pineda, and R. Powel, Phys. Rev. A **103**, 032806 (2021).